Exploratory Clinical Trial of (4S)-4-(3-[18F]fluoropropyl)-L-glutamate for Imaging xC− Transporter Using Positron Emission Tomography in Patients with Non–Small Cell Lung or Breast Cancer

Sora Baek[1], Chang-Min Choi[2], Sei Hyun Ahn[3], Jong Won Lee[3], Gyungyub Gong[4], Jin-Sook Ryu[1], Seung Jun Oh[1], Claudia Bacher-Stier[5], Lüder Fels[5], Norman Koglin[5], Christina Hultsch[5], Christoph A. Schatz[5], Ludger M. Dinkelborg[6], Erik S. Mittra[7], Sanjiv S. Gambhir[7,8], and Dae Hyuk Moon[1]

Abstract

Purpose: (4S)-4-(3-[18F]fluoropropyl)-L-glutamate (BAY 94-9392, alias [18F]FSPG) is a new tracer to image $x_C^−$ transporter activity with positron emission tomography (PET). We aimed to explore the tumor detection rate of [18F]FSPG in patients relative to 2-[18F]fluoro-2-deoxyglucose ([18F]FDG). The correlation of [18F]FSPG uptake with immunohistochemical expression of $x_C^−$ transporter and CD44, which stabilizes the xCT subunit of system $x_C^−$, was also analyzed.

Experimental Design: Patients with non–small cell lung cancer (NSCLC, $n = 10$) or breast cancer ($n = 5$) who had a positive [18F]FDG uptake were included in this exploratory study. PET images were acquired following injection of approximately 300 MBq [18F]FSPG. Immunohistochemistry was done using xCT- and CD44-specific antibody.

Results: [18F]FSPG PET showed high uptake in the kidney and pancreas with rapid blood clearance. [18F]FSPG identified all 10 NSCLC and three of the five breast cancer lesions that were confirmed by pathology. [18F]FSPG detected 59 of 67 (88%) [18F]FDG lesions in NSCLC, and 30 of 73 (41%) in breast cancer. Seven lesions were additionally detected only on [18F]FSPG in NSCLC. The tumor-to-blood pool standardized uptake value (SUV) ratio was not significantly different from that of [18F]FDG in NSCLC; however, in breast cancer, it was significantly lower ($P < 0.05$). The maximum SUV of [18F]FSPG correlated significantly with the intensity of immunohistochemical staining of $x_C^−$ transporter and CD44 ($P < 0.01$).

Conclusions: [18F]FSPG seems to be a promising tracer with a relatively high cancer detection rate in patients with NSCLC. [18F]FSPG PET may assess $x_C^−$ transporter activity in patients with cancer. *Clin Cancer Res; 18(19); 5427–37. ©2012 AACR.*

Introduction

One of the hallmarks of cancer is reprogramming energy metabolism (1). Cancer cells use both glucose and glutamine as a substrate to generate energy and to provide building blocks, such as amino acids, nucleosides, and fatty acids (2–4). Currently, increased glucose uptake and enhanced glycolytic metabolism of tumors is used for tumor positron emission tomography (PET) imaging with 2-[18F]fluoro-2-deoxyglucose ([18F]FDG). However, FDG has limitations in several tumor entities and settings. Therefore, imaging of other fundamental processes in tumors would be of great interest for early cancer detection, therapy monitoring, or prediction of resistance to chemotherapy (5).

The high rate of glucose and glutamine flux to increase cell mass results in an increase of oxidative intermediates, an altered redox potential, and excessive reactive oxygen species (3). Glutathione is the major thiol-containing endogenous antioxidant and serves as a redox buffer against various sources of oxidative stress (4, 6). The system $x_C^−$ is a heterodimeric transporter, composed of a light chain, xCT (SLC7A11), and heavy chain, 4F2hc (SLC3A2), which mediates the sodium-independent cellular uptake of cystine in exchange for intracellular glutamate at the plasma membrane (7). Intracellularly, cystine can then be converted to 2 molecules of cysteine, which is used for glutathione synthesis. Another main function of system $x_C^−$ is maintenance

Authors' Affiliations: Departments of [1]Nuclear Medicine, [2]Pulmonology, [3]Surgery, and [4]Pathology, Asan Medical Center, University of Ulsan College of Medicine, Seoul, Republic of Korea; [5]Bayer Pharma AG, Bayer Healthcare Pharmaceuticals; [6]Piramal Imaging, Berlin, Germany; [7]Molecular Imaging Program, Department of Radiology, Stanford Hospital and Clinics; and [8]Departments of Bioengineering and Materials Science & Engineering, Stanford University, Stanford, California

Corresponding Author: Dae Hyuk Moon, Department of Nuclear Medicine, Asan Medical Center, University of Ulsan College of Medicine, 86 Asanbyeongwon-gil, Songpa-gu, Seoul 138-736, Republic of Korea (South). Phone: 82-2-3010-4592; Fax: 82-2-3010-4588; E-mail: dhmoon@amc.seoul.kr

Translational Relevance

System x_C^- plays an important role in growth and progression of cancer and glutathione-based drug resistance. The xCT subunit of system x_C^- is stabilized by a splice variant of the cancer stem cell marker CD44 enabling better regulation of redox status in cancer cells. (4S)-4-(3-[18F]fluoropropyl)-L-glutamate ([18F]FSPG) is a novel 18F-labeled glutamate derivative for imaging of x_C^- transporter activity. In this study, we showed a high cancer detection rate of [18F]FSPG positron emission tomography (PET) with favorable biodistribution characteristics as a PET imaging tracer. Immunohistochemical staining indicated a correlation of [18F]FSPG uptake with the expression of the xCT subunit of system x_C^- together with CD44. Thus, we have shown a potential of [18F]FSPG PET imaging in assessing x_C^- transporter activity in tumor tissue noninvasively. [18F]FSPG PET imaging of system x_C^- activity might further improve the understanding of its role in cancer biology and chemoresistance in patients.

of a cysteine–cystine redox cycle in the extracellular compartments (8). In patients with cancer, it has become evident that the x_C^- transporter plays an important role in growth (9) and progression of cancer and glutathione-based drug resistance (10). CD44 is an adhesion molecule important for tumor cell invasion and metastasis and is a marker for cancer stem cells (11, 12). Quite recently, a CD44 splice variant has been reported to regulate redox status in cancer cells by stabilizing the xCT subunit of system x_C^- (13). (4S)-4-(3-[18F]fluoropropyl)-L-glutamate (BAY 94-9392, and herein referred to [18F]FSPG) is a novel 18F-labeled glutamate derivative for PET imaging. Specific transport of [18F]FSPG via the x_C^- transporter was shown in cell competition assays and xCT knockdown cells, and an excellent tumor visualization was achieved in animal tumor models (14). Tumor-specific adaptations of the intermediary metabolism and the function of system x_C^- and CD44 in glutathione biosynthesis and the cysteine–cystine redox cycle are schematically illustrated in Supplementary Fig. S1.

[18F]FSPG PET that examines x_C^- activity *in vivo* would provide information on oxidative stress of tumors and have a potential for the better understanding of tumor biology and chemoresistance mechanisms. The purpose of this study was to assess the tumor detection rate of [18F]FSPG PET in patients with lung or breast cancer relative to [18F]FDG. Furthermore, the dynamic biodistribution of [18F]FSPG in normal organs and tumors and the correlation of the uptake of [18F]FSPG with immunohistochemical staining intensity of xCT and CD44 were assessed.

Materials and Methods

Study design

This is an open-label, nonrandomized, single-dose explorative study conducted to evaluate the safety, tolerability, and diagnostic performance of [18F]FSPG positron emission tomography/computed tomography (PET/CT) in patients with non–small cell lung cancer (NSCLC) or breast cancer that showed lesions in previously conducted [18F]FDG PET/CT. The trial was registered at http://www.clinicaltrial.gov as NCT01103310. Primary outcome measure was visual assessment of the tumor detection rate with [18F]FSPG compared with that of [18F]FDG. The secondary outcome measures were quantitative analysis of [18F]FSPG uptake in tumors and assessment of safety variables including vital signs and laboratory findings. Effective radiation doses for [18F]FSPG as extrapolated from biodistribution studies in mice to humans were 5.1 mSv for a male and 6.5 mSv for a female subject (unpublished data). Our study protocol was approved by both the Institutional Review Board of the Asan Medical Center (University of Ulsan College of Medicine, Seoul, Republic of Korea) and the Korea Food and Drug Administration. This study was conducted in accordance with the Helsinki Declaration. All patients provided written informed consent before participation in the study.

Radiopharmaceutical preparation

Synthesis of the precursor and subsequent 18F labeling using 18F-fluoride were conducted as described recently (14). Each batch of [18F]FSPG that was produced met the criteria listed in the specification for appearance, identity, radiochemical and chemical purity, radioactivity concentration, specific activity, pH, bacterial endotoxin level, and sterility before being released. The final product was formulated as a sterile solution for intravenous injection. The amount of drug substance per injected unit was 300 ± 30 MBq and 100 μg or less mass dose. The specific activity was 18.2 GBq/μmol or more. The decay-corrected radiochemical yield was $29.1\% \pm 5.0\%$ (range, 20.5%–40.5%), and the radiochemical purity was $90.8\% \pm 0.5\%$ (range, 90.2%–91.6%).

Patients

The inclusion criteria consisted of patients who underwent [18F]FDG PET/CT and showed tumor mass with high certainty by visual analysis, histologically confirmed NSCLC or adenocarcinoma of the breast (female patients), age ≥35 and ≤75 years, an interval between [18F]FDG and [18F]FSPG PET/CT of 4 weeks or more, adequate recovery (excluding alopecia) from previous anticancer treatment, an Eastern Cooperative Oncology Group performance status of 0 to 2, and adequate function of major organs. No chemotherapy, radiotherapy or immune/biologic therapy, or biopsy were allowed between the [18F]FDG and the [18F]FSPG PET/CT. Patients were excluded from the study if any of the following applied to them: pregnancy, lactation, a concurrent, severe and/or uncontrolled, and/or unstable medical disease other than cancer, a lifetime history of alcohol or drug abuse, if they were a relative of any of the investigator, student of an investigator or a dependent, or if they were participating in or had participated in another clinical study involving the administration of an

investigational drug during the preceding 4 weeks. Patients were recruited by referral from investigators.

PET/CT procedure

[^{18}F]FDG PET/CT imaging was conducted as described previously (15). [^{18}F]FSPG PET/CT images were obtained using a PET/CT scanner (Biograph True Point 40 or Biograph 16; Siemens) on which [^{18}F]FDG PET/CT scans were acquired for clinical reasons. Oral hydration with water was encouraged, and no food restriction was required before [^{18}F]FSPG PET/CT studies. [^{18}F]FSPG PET/CT acquisition was conducted during 3 time intervals. The first interval ranged from 0 (immediately after tracer injection) to 45 minutes, the second interval from 60 to 75 minutes, and the third interval from 105 to 120 minutes. For attenuation correction of the PET scan, a low-dose CT (80 kV CARE Dose 4D, 31 mAs) without contrast medium administration was acquired for each imaging window. The total radiation exposure from the 3 CT examination did not exceed 3 mSv. Five, consecutive skull base-to-mid thigh or whole-body tumor imaging (top of the skull to the mid-thigh or feet) were acquired for the first imaging interval of 0 to 45 minutes along with the injection of 300 ± 10 MBq of [^{18}F]FSPG. Each PET scan was acquired for 0.5, 0.5, 1, 2, and 2 minutes per bed position, respectively. During the second and the third imaging intervals, 1 skull base-to-mid thigh or whole-body tumor image per each imaging window was acquired for 2 minutes per bed using the same acquisition parameter applied for the previous scan during the first imaging interval. Patients were asked to void their urinary bladder immediately after the first scan. Urinary bladder voiding was also encouraged before and after the second and third imaging session. Scans were corrected for random and scattered using the models implemented by the software supplied by the scanner manufacturer; they were also corrected for attenuation as estimated by the CT image. Data were reconstructed using the manufacturer-provided ordered-subset expectation maximization algorithm. No correction for partial volume effects was conducted.

Image analysis

The PET/CT studies were assessed visually and quantitatively by the consensus of 2 experienced nuclear medicine physicians who were informed of all available [^{18}F]FDG PET imaging, clinical, and laboratory findings. The readers reviewed all images to determine whether the image quality was adequate for interpretation. The number, location, size, extent, and intensity of all abnormal uptakes in relation to the background uptake in normal comparable tissues were described. Intensity features were classified as major, minor accumulation, or absent. Lesions with minor or major accumulation were regarded as positive. For dynamic assessment of [^{18}F]FSPG uptake in tumor and normal organs, spherical volumes of interest with a diameter of 1.5 or 1.2 cm were placed on normal organs and tumor, respectively. The selected tumor lesion was histologically proven to be cancer. A volume of interests on liver and descending thoracic aorta as the blood pool was drawn as previously

recommended (16). For quantitative analysis, the volume of interest was drawn semiautomatically using the vendor's software (TrueD, Siemens). Mean standardized uptake values (SUV_{mean}) of the volume of interest were obtained on each time frame to generate a time activity profile of the [^{18}F]FSPG uptake. All SUVs were normalized to the injected dose and the patients' body weight and were defined as follows:

$$SUV = activity \ (Bq/g)/[injected \ activity \ (Bq)/body \ weight \ (g)]$$

The [^{18}F]FSPG PET/CT image acquired 60 minutes after injection was used for visual and quantitative analysis. As many as 5 of the largest, malignant-looking lesions seen on [^{18}F]FDG PET/CT were selected and defined as reference lesions for lesion-based analysis and positive percentage agreement with [^{18}F]FSPG. Selected lesions were visually assessed with regard to their [^{18}F]FSPG uptake, which was then compared with that of [^{18}F]FDG. The maximal standardized uptake value (SUV_{max}) of each selected tumor lesion was measured using the single maximum pixel count within the lesion. The SUV ratio (SUVR) was obtained by calculating the ratio of the SUV_{max} of the tumor lesion and the SUV_{mean} of blood pool activity. Finally, the lesion detection rates of [^{18}F]FDG and [^{18}F]FSPG PET/CT were determined by measuring the total number of cancerous lesions using both [^{18}F]FDG and [^{18}F]FSPG PET/CT and based on subjective visual interpretation and available radiologic information.

The efficacy of [^{18}F]FSPG PET/CT was assessed in terms of patient-based as well as lesion-based detection, and histology served as the gold standard for patient-based sensitivity analysis. The positive percentage of agreement was calculated using positive [^{18}F]FDG uptake as a comparator. Additional lesion detection using [^{18}F]FSPG PET/CT was also analyzed.

Safety monitoring

For subjects enrolled, the safety of [^{18}F]FSPG was assessed on the basis of laboratory parameters (Supplementary Table S1), vital functions (blood pressure, heart beat, body temperature, etc.), electrocardiograms, and physical examinations at baseline, 2 hours after intravenous administration of [^{18}F]FSPG, and again at about 24 hours. Adverse events were continuously recorded, beginning with patient enrollment until the last patient contact between 3 to 8 days after [^{18}F]FSPG administration.

Immunohistochemistry of x_C^- transporter and CD44 expression

Tumor tissues from core-needle biopsies for routine diagnostic pathologic examinations were obtained before or after [^{18}F]FSPG PET/CT and used for immunohistochemistry (IHC) studies of x_C^- transporter and CD44. If patients underwent surgery after [^{18}F]FSPG PET/CT, this tumor specimen was used for further pathologic examination. A protocol for automatic immunohistochemical staining

device (Benchmark XT, Ventana Medical Systems) using formalin fixed, paraffin-embedded tissue sections was used. Briefly, 4-µm thick whole tissue sections were transferred onto poly-L-lysine–coated adhesive slides and dried at 74°C for 30 minutes. After standard heat epitope retrieval for 1 hour in EDTA, pH 8.0, in the autostainer, the samples were incubated with antibodies to both of the x_C^- transporter (1:250 dilution; NB300-318, polyclonal anti-xCT antibody, Novus Biologicals; ref. 17), and CD44 (1:100 dilution; Clone DF 1485, DakoCytomation). The sections were subsequently incubated with ultraView Universal DAB kit (Ventana Medical Systems). Slides were counterstained with Harris hematoxylin. Pancreatic tissue and tissue microarrays of variable cancer tissues including breast and lung were used as positive controls for xCT and tonsil for positive CD44 controls. Incubation with the primary antibody was omitted in the negative controls. The level of expression of x_C^- transporter in both membrane and cytoplasm and of CD44 in the membrane of malignant tumor cells was examined by an experienced pathologist who was completely blinded to any patient and imaging information. The results of the immunoassay for x_C^- transporter and CD44 were semiqualitatively assessed using a scale of 0, 1+ (weak), 2+ (medium), and 3+ (strong) with a sample being reported as positive if greater than 10% of the cells in the sample were positively stained. The correlation between the intensity of immunohistochemical staining and SUV_{max} of the corresponding lesion on the PET/CT was then assessed.

Statistical analysis

Data were reported as mean $\pm$ SD unless otherwise specified. A P value of <0.05 was considered to be statistically significant. Comparison of quantitative parameters was conducted using the paired t test. The correlation of [^{18}F]FSPG uptake (SUV_{max}) with the intensity of x_C^- transporter and CD44 IHC was assessed using Spearman rank correlation coefficients (ρ). The significance level was calculated assuming that t [$t = rs\sqrt{[(n-2)/(1-rs^2)]}$ in which rs is the sample Spearman rank correlation coefficient] is distributed approximately as Student t distribution with $n - 2$ degrees of freedom under the null hypothesis. All statistical tests were conducted using the IBM SPSS Statistics Version 19 for Windows (SPSS, Inc., IBM Company).

Results

Patients and [^{18}F]FSPG PET/CT procedure

Among patients assessed for eligibility, 1 patient with NSCLC declined to participate before receiving [^{18}F]FSPG injection and was replaced by an additional patient. Ten patients with NSCLC and 5 with breast cancer were included in this study and were examined at Asan Medical Center between April 2010 and December 2010 (8 men, 7 women; ages 35–70 years). All but 1 patient (patient 10 in Table 1) was examined on a Biograph True Point 40 scanner. [^{18}F]FSPG PET/CT studies were completed without any scanner- or patient-related problems. The mean time inter-

val between [^{18}F]FDG and [^{18}F]FSPG PET/CT was 2.7 $\pm$ 3.7 days (range, 1–12 days). The patient and lesion characteristics are listed in Table 1. All but 2 patients were newly diagnosed as NSCLC or breast cancer. Patient 14 had right modified radical mastectomy followed by adjuvant chemotherapy 3 years ago. Local recurrent lesions were treated with mass excision and radiotherapy 4 months before the enrollment. Patient 15 underwent skin-sparing mastectomy for primary breast cancer 2 years ago. Both patients were on hormonal treatment. All patients void their urinary bladder immediately after the first imaging session. All [^{18}F]FSPG PET/CT procedures were conducted as planned.

Safety

Administration of [^{18}F]FSPG and the PET/CT procedures were well tolerated by all 15 patients. No clinically relevant changes in safety parameters were observed. There were no study drug–related adverse events.

Biodistribution of [^{18}F]FSPG

The overall image quality was adequate for diagnosis in all patients, and all patients showed initially high uptake in the kidneys and pancreas. The kidneys showed a rapid, intense uptake, which gradually decreased (11.1 $\pm$ 1.5 SUV_{mean} at 60 minutes postinjection), whereas the pancreas and scalp activity continuously increased, reaching a plateau at approximately 15 to 60 minutes postinjection (SUV_{mean} value determined at 60 minutes for the pancreas was 8.6 $\pm$ 4.5 and the scalp 2.0 $\pm$ 0.5, respectively). This uptake and excretion pattern resulted in prominent signals from the kidney, pancreas, and bladder, as seen on delayed images (Fig. 1). Liver, breast, and bone marrow showed prolonged uptake, which resulted in normal visualization on delayed images. [^{18}F]FSPG cleared rapidly from the blood pool with 0.8 $\pm$ 0.2 SUV_{mean} of blood pool activity 60 minutes following injection. However, vascular activity was visible on the most of the PET acquisitions but was then barely distinguishable from the low-level background activity 105 minutes following injection (SUV_{mean}, 0.4 $\pm$ 0.1). No focal or elevated uptake was observed in the brain, muscle, small or large intestinal track, or on the cortical or trabecular bone surfaces. In some patients, delayed activity accumulation in the stomach was observed.

[^{18}F]FSPG tumor uptake

The size of histologically proven NSCLC or breast cancer for dynamic assessment of [^{18}F]FSPG uptake was 3.9 $\pm$ 2.4 cm. Tumor activity continuously increased, reaching a plateau at about 60 minutes. There were large variations in the SUV_{mean} among individual patients and in different tumor types (NSCLC: 5.4 $\pm$ 4.8; breast: 1.8 $\pm$ 1.2 at 60 minutes postinjection). Because of the clearance of background activity over time, the tumor-to-background ratios of 1 representative lesion increased over time up to 105 minutes (tumor/blood ratio of SUV_{mean}: 5.7 $\pm$ 5.4 at 60 minutes postinjection and 9.2 $\pm$ 9.0 at 105 minutes postinjection). For more detailed information, see Supplementary Table S2 and Supplementary Fig. S2.

Table 1. Characteristics of patients and their reference lesions on [^{18}F]FDG and [^{18}F]FSPG PET/CT and IHC intensity scores for x_C^- and CD44

Patient	Age (y)	Sex	Pathology	Location	SUV$_{max}$ at 60 minutes		IHC intensity	
					FDG	FSPG	x_C^-	CD44
1	68	M	NSCLC, adenocarcinoma	Right lung	14.7	7.3	2	1
2	58	F	NSCLC, adenocarcinoma	Right lung	25.8	22.5	3	3
				Lymph node	18.5	14.8		
				Lymph node	19.9	26.3		
				Lymph node	12.7	19.5		
				Lymph node	10.9	20.7		
3	70	M	NSCLC, squamous cell carcinoma	Right lung	13.5	11.4	2	3
				Right lung	11.2	4.2		
4	54	M	NSCLC, adenocarcinoma	Right lung	9.1	1.4	NA	NA
				Right lung	4.2	0.5[c]		
				Lymph node	5.4	1.4[c]		
				Lymph node	4.8	2.8		
				Bone	12.5	2.4		
5	66	M	NSCLC, adenocarcinoma	Right lung	18.5	1.6	2	2
6	60	M	NSCLC, squamous cell carcinoma.	Left lung	21.0	13.0	NA	NA
				Lymph node	16.9	9.3		
				Lymph node	28.4	14.9		
				Lymph node	18.7	6.0		
				Lymph node	23.6	9.0		
7	50	F	NSCLC, adenocarcinoma	Right lung	14.3	4.6	3	2
				Lymph node	9.0	2.8		
				Lymph node	3.4	1.8		
8	54	M	NSCLC, adenocarcinoma	Lymph node	11.4	2.3		
				Brain	5.4[a]	3.8		
				Lymph node	7.2	2.3		
				Lymph node	11.2	2.1	2	NA[b]
				Lymph node	8.6	1.9		
9	62	M	NSCLC, adenocarcinoma	Right lung	16.4	12.3	3	3
10	55	M	NSCLC, adenocarcinoma	Right lung	9.2	3.9	3	1
				Lymph node	3.3	2.5		
11	37	F	Breast, invasive ductal carcinoma	Left breast	11.8	2.1[c]	2	0
				Lymph node	9.0	2.2		
				Lymph node	8.8	1.7		
12	45	F	Breast, invasive ductal carcinoma	Left breast	7.3	1.3[c]	2	0
				Lymph node	4.0	0.9		
				Lymph node	3.6	0.9		
				Lymph node	2.3	1.3		
				Lymph node	2.0	0.8		
13	40	F	Breast, invasive ductal carcinoma	Right breast	38.0	3.5	2	0
				Lymph node	27.5	2.1		
				Lymph node	12.2	1.7		
				Lymph node	10.3	1.8		
				Lymph node	13.5	2.1		
14	53	F	Breast, metastatic ductal carcinoma	Liver	9.1	7.7	3	3
15	54	F	Breast, invasive ductal carcinoma	Bone	29.7	2.1		
				Right breast	23.3	1.6	0	0
				Bone	44.3	1.9		
				Lymph node	17.8	1.9		
				Liver	7.0	2.0[c]		

Abbreviation: NA, not assessed.
[a]Brain imaging 10 hours after [^{18}F]FDG administration.
[b]Not possible with biopsy sample.
[c]Lesions that were visually interpreted as negative. Other lesions were positive by visual assessment.
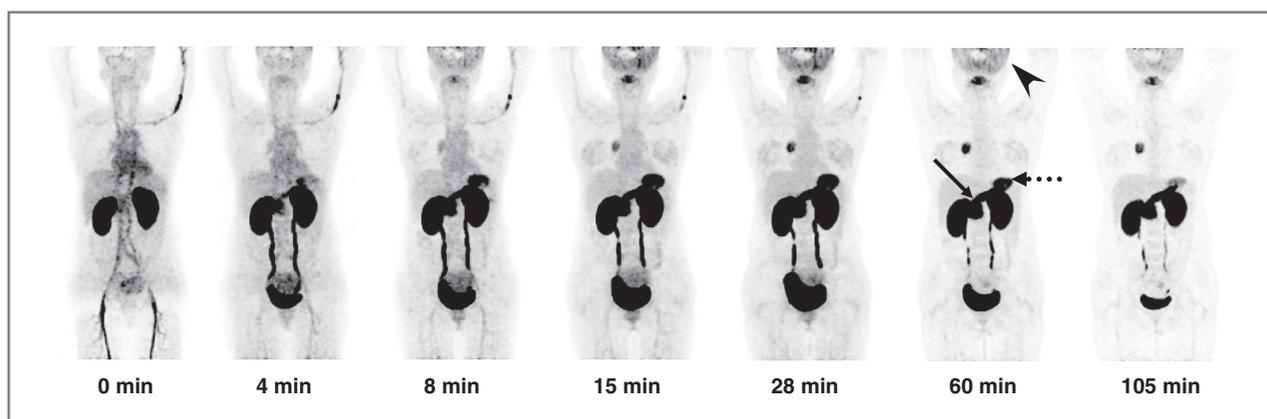
Figure 1. Anterior maximum intensity projections of [^{18}F]FSPG PET at 0, 4, 8, 15, 28, 60, and 105 minutes after injection (from left to right), in a patient with lung cancer (patient 7). The intensity scale was adjusted at the same level for all images. The kidney shows a rapid intense uptake. The pancreas (arrow) and scalp (arrow head) activity increases continuously, reaching a plateau at approximately 15 to 60 minutes. Tumor activity in the right lower lobe of the lung increases continually, reaching a plateau at about 60 minutes. Delayed activity accumulation in the stomach was observed in some patients, as seen in this patient (dotted arrow).

The results of the visual and quantitative analysis of [^{18}F]FSPG PET are summarized in Table 2. All 10 NSCLC and 3 of the 5 breast cancer lesions that were confirmed by pathology examination could also be visually identified by [^{18}F]FSPG PET. Two missed breast cancer lesions were sized more than 7 cm and were identified by clinical examination and conventional imaging studies. Thirty lesions with NSCLC and 19 with breast cancer were selected as reference. The size of these reference lesions of patients with NSCLC or breast cancer for lesion-based analysis was 2.6 ± 1.6 cm and 2.8 ± 2.2 cm, respectively. We included 1 brain lesion that was scanned 10 hours after FDG injection under the principle of intention-to-diagnose (patient 8). The visually assessed signal intensity activity of [^{18}F]FSPG accumulation was the same as that of [^{18}F]FDG in 70% (21/30) of the reference lesions in patients with NSCLC (Fig. 2 and Supplementary Movie S1). However, with breast cancer, only 11% (2/19) of the lesions showed the same uptake visually (Fig. 3), whereas 89% (17/19) of the lesions had lower [^{18}F]FSPG accumulation (Table 1). In the NSCLC patient group, only 1 lesion was better visualized on [^{18}F]FSPG than on [^{18}F]FDG PET (brain metastasis). When the total number of cancerous lesions using both [^{18}F]FDG and [^{18}F]FSPG PET/CT were compared, [^{18}F]FSPG detected 59 of 67 (88%) positive [^{18}F]FDG lesions in NSCLC, and 30 of 73 (41%) in breast cancer. Seven lesions (brain 1, pleura 3,

Table 2. Visual and quantitative analysis of [^{18}F]FSPG PET compared with [^{18}F]FDG PET

Visual analysis			Cancer	
Subject	**Comparator**	**Efficacy variable**	**Lung**	**Breast**
Patient	Pathology	Sensitivity	100% (10/10)	60% (3/5)
Reference lesions defined by	[^{18}F]FDG uptake	Higher [^{18}F]FSPG	3% (1/30)	0% (0/19)
positive uptake on [^{18}F]FDG PET (≤5 per patient)		Same [^{18}F]FSPG	70% (21/30)	11% (2/19)
		Lower [^{18}F]FSPG	27% (8/30)	89% (17/19)
Total lesions on [^{18}F]FDG	[^{18}F]FDG	Percent agreement	88% (59/67)	41% (30/73)
New lesions on [^{18}F]FSPG	[^{18}F]FDG	N of new lesions	7 in 2 patients	0

Quantitative analysis			Cancer	
Subject	**Variables**	**PET tracer**	**Lung ($n = 30$)**	**Breast ($n = 19$)**
Reference lesions defined by	SUV$_{max}$	[^{18}F]FDG	13.0 ± 6.7	14.8 ± 1.2
positive uptake on [^{18}F]FDG PET (≤5 per patient)		[^{18}F]FSPG	7.6 ± 7.3[a]	2.1 ± 1.5[a]
	SUVR	[^{18}F]FDG	7.7 ± 4.2	8.9 ± 7.9
		[^{18}F]FSPG	9.7 ± 8.6[b]	3.6 ± 5.4[c]

[a]$P < 0.001$ between [^{18}F]FDG and [^{18}F]FSPG.
[b]P = not significant between [^{18}F]FDG and [^{18}F]FSPG.
[c]$P < 0.05$ between [^{18}F]FDG and [^{18}F]FSPG.

Figure 2. A 58-year-old female patient with multiple metastatic lesions from NSCLC (patient 2). Maximum-intensity projection of [^{18}F]FDG (A) and [^{18}F]FSPG (B) PET/CT show metastatic lesions in lung, pleura, lymph nodes, bone, and pancreas. Note that the lesions in lung, pleura, and supraclavicular lymph node are evident only on [^{18}F]FSPG PET (arrows), whereas the metastatic lesion in the pancreas (arrow head) is not seen due to the normal high pancreatic uptake. In contrast to [^{18}F]FDG, no uptake of [^{18}F]FSPG is observed in the brain. Immunohistochemical evaluation of x_C^- (C, ×400) and CD44 (D, ×400) shows intense staining (3+) in the cell membrane (x_C^- and CD44) and cytoplasm (x_C^-) of the primary lung lesion.
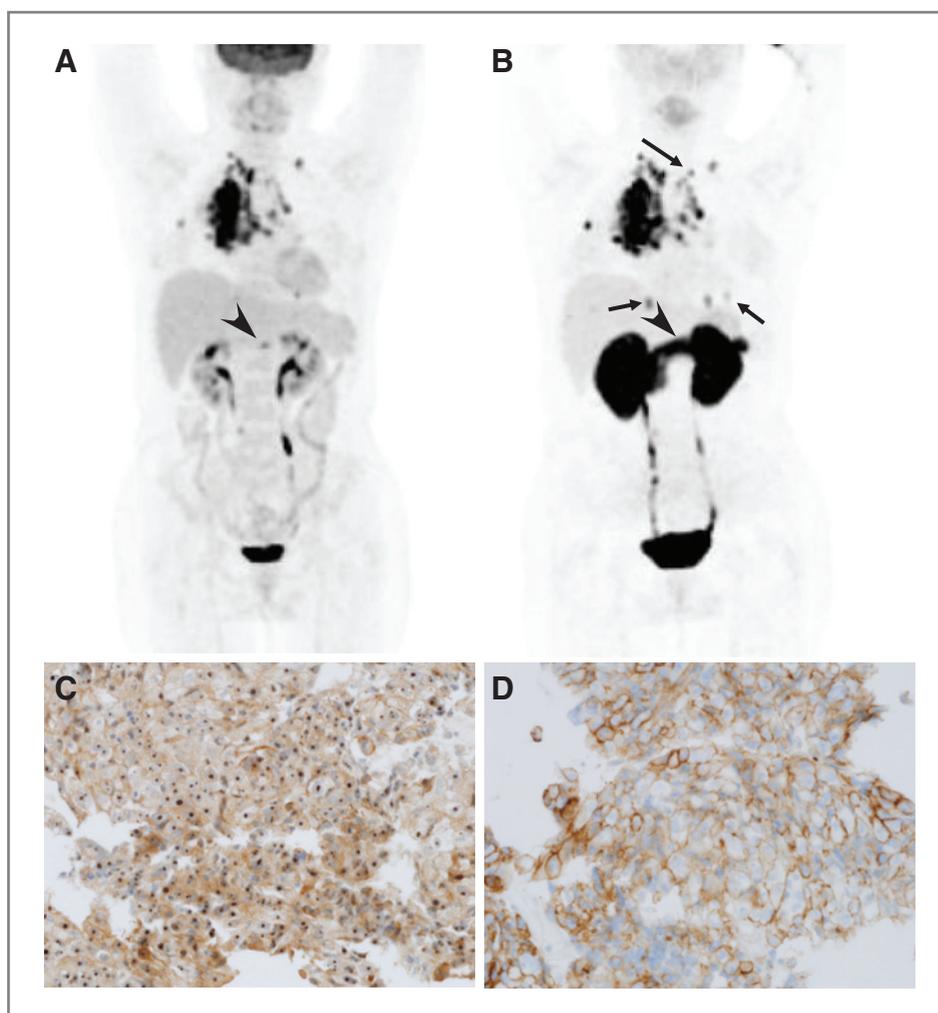
lung 2, and lymph node 1) were additionally detected only on [^{18}F]FSPG in 2 patients with NSCLC (Fig. 2). Pathologic diagnosis of the additional lesions on [^{18}F]FSPG PET was not made, but MRI and chest CT revealed 3 metastatic lesions in the brain, lung, and supraclavicular lymph node station.

Figure 3. Transaxial [^{18}F]FDG (A), [^{18}F]FSPG PET/CT (B), contrast enhanced CT (C), and T1-weighted magnetic resonance image (D) of a 53-year-old female patient with metastatic ductal carcinoma in the caudate lobe of the liver (patient 14). A 6 mm metastatic nodule is seen on [^{18}F]FDG (A) and [^{18}F]FSPG (B) PET/CT, although there is no visible lesion on contrast-enhanced CT scans at the same level (C). The corresponding T1-weighted MRI shows a small, low-signal-intensity lesion (D). Immunohistochemical evaluation of x_C^- (E, ×400) and CD44 (F, ×400) shows intense staining (3+) in the cell membrane (x_C^- and CD44) and cytoplasm (x_C^-) of the metastatic lesion in the liver.
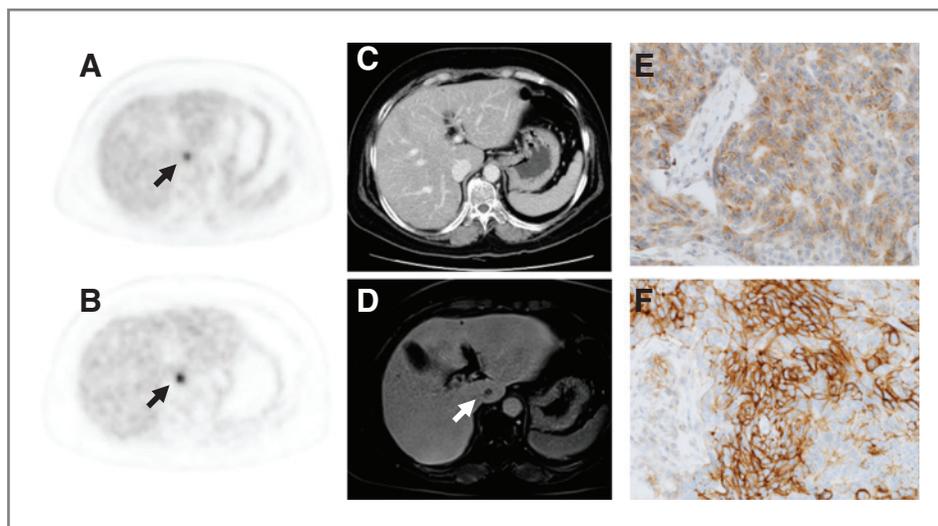
Quantitative analysis of [18F]FSPG also showed similar findings. The SUV_{max} of tumor lesions was significantly higher for [18F]FDG PET than that for [18F]FSPG PET in NSCLC and breast cancer ($P < 0.001$, Table 2). There was a modest correlation between SUV_{max} of [18F]FDG and [18F]FSPG (NSCLC, $\rho = 0.69$, $P < 0.001$; breast cancer, $\rho = 0.61$, $P < 0.005$; Supplementary Fig. S3). The SUVR of NSCLC were comparable ($P = 0.12$), although in breast cancer, the SUVR of [18F]FDG differed significantly from that of [18F]FSPG ($P < 0.05$, Table 2). For more information on a patient with low [18F]FSPG uptake, see the Supplementary Fig. S4 and Supplementary Movie S2.

[18F]FSPG uptake and correlation with immunohistochemical staining of xCT and CD44

The mean time interval between [18F]FSPG PET/CT and surgery or biopsy for routine diagnostic pathologic study was 2.5 ± 11.0 days. Immunohistochemical staining of tumors revealed that 12 patients had x_C^- transporter-positive tumors (8 NSCLC and 4 breast cancer, 7 with 2+ immunostaining, and 5 with 3+ immunostaining). In 1 patient with breast cancer, no x_C^- transporter expression was identified (Table 1). [18F]FSPG SUV_{max} values at 60 minutes after injection showed high variability and overlapped between tumors with 2+ score (range, 1.3–11.4) and 3+ (range, 3.9–22.5, Fig. 4A). Samples from 4 patients with breast cancer showed lowest [18F]FSPG uptake ($SUV_{max} < 5$) despite a xCT 2+ immunostaining score. Among 12 patients, 8 had CD44-positive tumors (7 NSCLC and 1 breast cancer; 2 with 1+, 2 with 2+, and 4 with 3+ immunostaining) and 4 patients with breast cancer had CD44-negative tumors. Tumors with CD44 3+ immunostaining showed highest [18F]FSPG SUV_{max} values at 60 minutes, whereas CD44 0 to 2+ immunostaining resulted in lower SUV_{max} values (Fig. 4B). Statistical analyses revealed a significant correlation of [18F]FSPG SUV_{max} 60 minutes after injection with both x_C^- transporter ($\rho = 0.68$, $P < 0.01$) and CD44 expression ($\rho = 0.77$, $P < 0.01$, Fig. 4). SUVR also correlated with immunohistochemical staining results in the same manner (data not shown). A significant correlation was also observed between immunohistochemical staining of xCT and CD44 as shown in Supplementary Fig. S5 ($\rho = 0.65$, $P < 0.05$). Two patients with NSCLC and 1 patient with breast cancer (liver metastasis) with both strong positive xCT and CD44 expression showed a very high [18F]FSPG SUV_{max}, as seen in Figs. 2 and 3, whereas 1 with both negative immunohistochemical staining had a low SUV_{max} (patient 15). All patients with negative CD44 showed a low [18F]FSPG SUV_{max} of ≤ 4.0 (patient 11, 12, 13, and 15). No significant relationship was observed between [18F]FDG and immunohistochemical staining scores of xCT and CD44.

Discussion

The data reported in this manuscript are the first human data on [18F]FSPG in patients with NSCLC or breast cancer. [18F]FSPG showed a favorable biodistribution and clearance pattern allowing its use as a potential PET tracer in
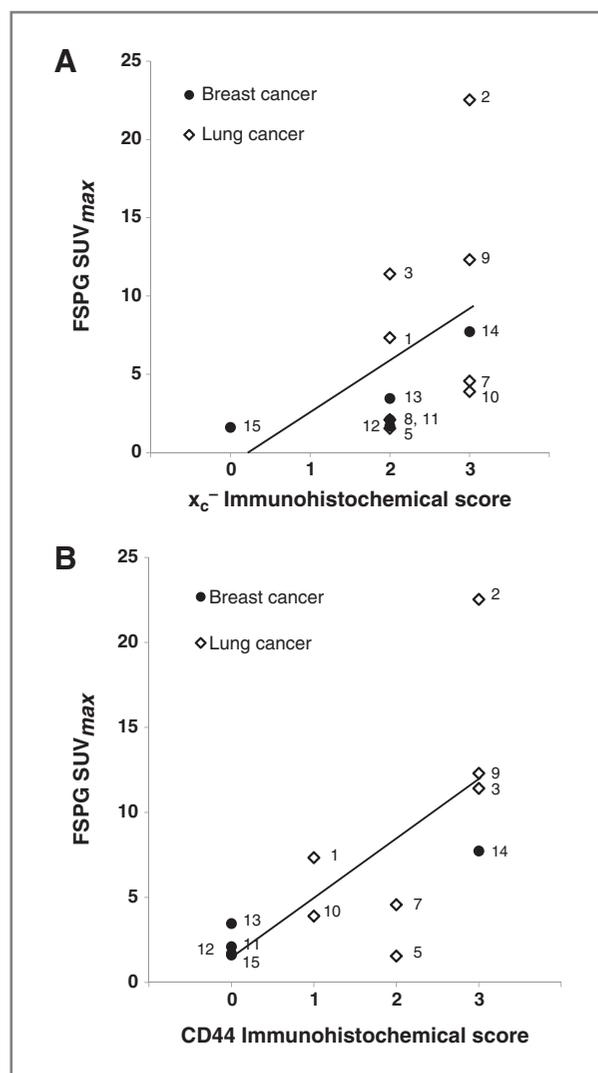

Figure 4. The relationship between [18F]FSPG SUV_{max} and the staining intensity of x_C^- transporter (A) and CD44 (B) expression. The SUV_{max} of [18F]FSPG correlates significantly with the intensity of immunohistochemical staining of x_C^- transporter ($\rho = 0.68$, $P < 0.01$) and CD44 ($\rho = 0.65$, $P < 0.05$). The data points are labeled with the respective patient number (Table 1).

patients with cancer. [18F]FSPG showed a relatively high tumor detection rate and high tumor to background ratios that were comparable with that of [18F]FDG in NSCLC but not in breast cancer. Particularly, additional lesions not seen on [18F]FDG were detected by [18F]FSPG in patients with NSCLC. We found that [18F]FSPG was well tolerated, safe, and without adverse events in all 15 study patients. Correlation of [18F]FSPG uptake with the staining intensity of 2 immunohistochemical markers (xCT and CD44) suggests the potential ability of [18F]FSPG PET to assess the system x_C^- activity in patients with cancer.

The biodistribution data showed increasing uptake up to 60 minutes after injection in pancreas and scalp, whereas predominant renal excretion resulted in high initial uptake in the kidneys, which decreased slowly over time. In human

studies of a wide variety of tissues and cells examined, x_C^- transporter is predominantly expressed in the brain, pancreas (18), stromal, and immune cells. In monkeys, xCT protein distribution was shown in the kidney and duodenum (19). A recent study suggests that the *Slc7a11* gene is a major genetic regulator of pheomelanin in hair and melanocytes (20). The critical role of x_C^- transporter in the control of pigmentation may correspond with the scalp uptake of [18F]FSPG in this study. Our biodistribution data are therefore in accordance with previous studies with xCT and [18F]FSPG biodistribution in animals (14). No uptake in healthy brain tissue is likely due to inability of the tracer to cross the intact blood brain barrier. High normal uptake in the pancreas and kidneys and excretion in bladder likely precludes the use of [18F]FSPG in assessing tumors in these organs, as shown in Fig. 2. However, low background in other organs is very advantageous in detecting lesions, especially in the abdomen and brain in which [18F]FDG PET has limitations in differentiating tumor from normal uptake. In addition, low bone uptake of [18F]FSPG was observed, which might be useful for the assessment of metastatic bone lesions. An accompanying study to assess biodistribution, stability, and radiation dosimetry of [18F]FSPG in healthy volunteers showed that the critical organs for the radiation dose were the kidney and the urinary bladder wall followed by the pancreas (Smolarz et al., manuscript in preparation). The effective dose of [18F]FSPG was slightly lower than that of [18F]FDG. Only the parent compound was detected by analysis of blood samples from healthy volunteers for up to 4 hours postinjection indicating high stability of the compounds in humans (unpublished data; Smolarz et al., manuscript in preparation).

Although, time–activity curve of tumor SUV showed variable patterns, the average tumor uptake of [18F]FSPG increased until 60 minutes and remained constant over the following study period. Tumor to background ratio increased over the time up to 105 minutes, as background SUV decreased more rapidly than that of tumors during the whole imaging period. As tumor detection rates of [18F]FSPG images obtained after 60 and 105 minutes were the same (data not shown), and [18F]FDG PET 60 minutes after injection was used as a comparator, we selected the 60-minute images of [18F]FSPG for further analysis. Our data showed that tumor uptake and tumor detection rate of [18F]FSPG was remarkably high in NSCLC but lower in breast cancer. A positive [18F]FDG PET scan was an inclusion criteria for patients in this study. Thus, no conclusions in terms of superiority/inferiority can be drawn from this study, and further studies with [18F]FSPG in an unselected patient cohort are needed. As [18F]FSPG targets a completely different metabolic pathway than glycolysis, tumors with a high rate of glycolysis do not have to be necessarily avid for [18F]FSPG in parallel. Nevertheless, in NSCLC, a high degree of overlap between tumors with a high glycolytic phenotype and [18F]FSPG-positive phenotype was observed, whereas [18F]FDG-positive tumors in breast cancer showed lower detection rate and accumulation of [18F]FSPG. More studies in NSCLC, breast cancer subtypes, and other cancer indica-

tions are needed to further elucidate and define the future role of [18F]FSPG.

Our results showed higher [18F]FSPG uptake in patients with NSCLC but substantially lower in patients with breast cancer. Cancer cells may possibly use alternative pathways to ensure cysteine availability in the absence of x_C^- transporter. For example, cysteine can be synthesized from L-methionine via the transsulfuration pathway as shown in C6 glioma cells (21). NCI60 panel studies revealed that the expression level of cystathionine β-synthase, the key enzyme of the transsulfuration pathway, is the highest in breast cancer cell lines but lower in lung cancer cell lines (22). Another pathway for cysteine availability is the γ-glutamyl cycle, which allows the efficient use of glutathione for cysteine storage (23). Altered expression of γ-glutamyl transpeptidase has been found in human tumors of the liver, lung, and breast (24, 25). Fibroblasts, activated macrophages, or dendritic cells may also supply cancer cells with cysteine as shown in lymphoid cells, which are unable to express the system x_C^- (26, 27). These cells may take up cystine from the extracellular space by using the system x_C^- transporter, convert cystine to cysteine intracellularly, and release cysteine into the extracellular space, where it is available to cancer cells via transporters, such as those from the alanine-serine-cysteine family. All these mechanisms may partially explain the observed differences in [18F]FSPG uptake between NSCLC and patients with breast cancer. The relative contribution of different mechanisms for cysteine availability needs to be further explored.

Our data showed that even a 2+ immunostaining score for xCT does not necessarily result in a high [18F]FSPG uptake. Meanwhile, all patients with negative xCT or CD44 had a low level of [18F]FSPG uptake. Interestingly, 3 patients with both strong positive xCT and CD44 expression showed a very high [18F]FSPG SUV_{max}. All these findings suggest a relationship of [18F]FSPG uptake with the staining intensity of IHC if both the xCT subunits of system x_C^- and CD44 are considered. A recent study reported a role of a CD44 splice variant in regulating the redox status in cancer cells by stabilizing the xCT subunit at the cell membrane (13). Although the CD44 antibody used in this study is not able to distinguish between normal and the CD44 splice variant, the CD44 splice variant can be assumed to be the dominant CD44 form in tumors (28). Our results may confirm an important role of CD44 for the proper functioning of the system x_C^-. However, IHC data show only protein expression and does not provide any information on the functional activity, which is of great importance when studying transporter molecules. Staining of the xCT subunit was observed in the membrane and/or cytosol. No relationship was found between [18F]FSPG uptake and localization of xCT staining. In addition, we may not explain a low level of [18F]FSPG uptake even though with positive xCT 2+ and CD44 2+ immunostaining in patient 5. We need more studies to clarify these issues. IHC using a specific antibody to the CD44 splice variant may help to better understand this situation.

A small number of patients and the exploratory nature of this study limit its statistical power. Validation of [^{18}F]FSPG in a different patient population with further refinements in quantitative PET measurement (29) and IHC (30) is therefore needed. In addition, patients were not fasted before the [^{18}F]FSPG PET. In view of similar affinities of cystine and glutamate for x_C^- transporter, plasma cystine or glutamate may potentially inhibit [^{18}F]FSPG uptake (14, 31). However, overall postprandial changes were reported to be small, and peak levels are expected to be less than 100 µmol/L (32–34). We believe that the nonfasting status did not affect the [^{18}F]FSPG uptake significantly in most patients. Finally, tumors sometimes show high heterogeneity, and immunohistochemical staining of tumor biopsy samples will show different results compared with PET imaging in which the entire tumor lesion is measured. Further studies will further examine the heterogeneity of system x_C^- expression across the tumor bed and might better explain sometime discordant imaging results.

In conclusion, [^{18}F]FSPG is safe and seems to be a promising novel tumor imaging agent with a favorable biodistribution and high cancer detection rate in patients with NSCLC. [^{18}F]FSPG PET imaging may assess x_C^- transporter activity in tumor tissue noninvasively. A significant correlation between [^{18}F]FSPG and xCT as well as CD44 using IHC suggests a role in the assessment of oxidative stress–induced signaling, which may lead to a better understanding of chemoresistance mechanisms. Given that CD44 has broad functions in cellular signaling cascades (12), additional roles of [^{18}F]FSPG PET are expected. More studies are needed to elucidate a correlation with tumor progression, metastasis, and chemoresistance, which may provide more insights into potential clinical applications of this new tumor PET tracer.

References

1. Hanahan D, Weinberg RA. Hallmarks of cancer: the next generation. Cell 2011;144:646–74.
2. Vander Heiden MG, Cantley LC, Thompson CB. Understanding the Warburg effect: the metabolic requirements of cell proliferation. Science 2009;324:1029–33.
3. Levine AJ, Puzio-Kuter AM. The control of the metabolic switch in cancers by oncogenes and tumor suppressor genes. Science 2010;330:1340–4.
4. DeBerardinis RJ, Cheng T. Q's next: the diverse functions of glutamine in metabolism, cell biology and cancer. Oncogene 2010;29:313–24.
5. Mankoff DA, Eary JF, Link JM, Muzi M, Rajendran JG, Spence AM, et al. Tumor-specific positron emission tomography imaging in patients: [18F] fluorodeoxyglucose and beyond. Clin Cancer Res 2007;13:3460–9.
6. Estrela JM, Ortega A, Obrador E. Glutathione in cancer biology and therapy. Crit Rev Clin Lab Sci 2006;43:143–81.
7. Sato H, Tamba M, Ishii T, Bannai S. Cloning and expression of a plasma membrane cystine/glutamate exchange transporter composed of two distinct proteins. J Biol Chem 1999;274:11455–8.
8. Banjac A, Perisic T, Sato H, Seiler A, Bannai S, Weiss N, et al. The cystine/cysteine cycle: a redox cycle regulating susceptibility versus resistance to cell death. Oncogene 2008;27:1618–28.
9. Lyons SA, Chung WJ, Weaver AK, Ogunrinu T, Sontheimer H. Autocrine glutamate signaling promotes glioma cell invasion. Cancer Res 2007;67:9463–71.
10. Huang Y, Dai Z, Barbacioru C, Sadee W. Cystine-glutamate transporter SLC7A11 in cancer chemosensitivity and chemoresistance. Cancer Res 2005;65:7446–54.
11. Ponta H, Sherman L, Herrlich PA. CD44: from adhesion molecules to signalling regulators. Nat Rev Mol Cell Biol 2003;4:33–45.
12. Zoller M. CD44: can a cancer-initiating cell profit from an abundantly expressed molecule? Nat Rev Cancer 2011;11:254–67.
13. Ishimoto T, Nagano O, Yae T, Tamada M, Motohara T, Oshima H, et al. CD44 variant regulates redox status in cancer cells by stabilizing the xCT subunit of system xc(−) and thereby promotes tumor growth. Cancer Cell 2011;19:387–400.
14. Koglin N, Mueller A, Berndt M, Schmitt-Willich H, Toschi L, Stephens AW, et al. Specific PET imaging of xC− transporter activity using a (1)F-labeled glutamate derivative reveals a dominant pathway in tumor metabolism. Clin Cancer Res 2011;17:6000–11.
15. Yoon DH, Baek S, Choi CM, Lee DH, Suh C, Ryu JS, et al. FDG-PET as a potential tool for selecting patients with advanced non–small cell lung cancer who may be spared maintenance therapy after first-line chemotherapy. Clin Cancer Res 2011;17:5093–100.

16. Wahl RL, Jacene H, Kasamon Y, Lodge MA. From RECIST to PERCIST: evolving considerations for PET response criteria in solid tumors. J Nucl Med 2009;50 Suppl 1:122S–50S.

17. Liu R, Blower PE, Pham AN, Fang J, Dai Z, Wise C, et al. Cystine-glutamate transporter SLC7A11 mediates resistance to geldanamycin but not to 17-(allylamino)-17-demethoxygeldanamycin. Mol Pharmacol 2007;72:1637–46.

18. Bassi MT, Gasol E, Manzoni M, Pineda M, Riboni M, Martin R, et al. Identification and characterisation of human xCT that co-expresses, with 4F2 heavy chain, the amino acid transport activity system xc. Pflugers Arch 2001;442:286–96.

19. Burdo J, Dargusch R, Schubert D. Distribution of the cystine/glutamate antiporter system xc− in the brain, kidney, and duodenum. J Histochem Cytochem 2006;54:549–57.

20. Chintala S, Li W, Lamoreux ML, Ito S, Wakamatsu K, Sviderskaya EV, et al. Slc7a11 gene controls production of pheomelanin pigment and proliferation of cultured cells. Proc Natl Acad Sci U S A 2005;102:10964–9.

21. Kandil S, Brennan L, McBean GJ. Glutathione depletion causes a JNK and p38MAPK-mediated increase in expression of cystathionine-gamma-lyase and upregulation of the transsulfuration pathway in C6 glioma cells. Neurochem Int 2010;56:611–9.

22. Zhang W, Braun A, Bauman Z, Olteanu H, Madzelan P, Banerjee R. Expression profiling of homocysteine junction enzymes in the NCI60 panel of human cancer cell lines. Cancer Res 2005;65:1554–60.

23. Hanigan MH. Expression of gamma-glutamyl transpeptidase provides tumor cells with a selective growth advantage at physiologic concentrations of cyst(e)ine. Carcinogenesis 1995;16:181–5.

24. Hanigan MH, Frierson HF Jr, Swanson PE, De Young BR. Altered expression of gamma-glutamyl transpeptidase in human tumors. Hum Pathol 1999;30:300–5.

25. Hochwald SN, Harrison LE, Rose DM, Anderson M, Burt ME. Gamma-glutamyl transpeptidase mediation of tumor glutathione utilization in vivo. J Natl Cancer Inst 1996;88:193–7.

26. Angelini G, Gardella S, Ardy M, Ciriolo MR, Filomeni G, Di Trapani G, et al. Antigen-presenting dendritic cells provide the reducing extracellular microenvironment required for T lymphocyte activation. Proc Natl Acad Sci U S A 2002;99:1491–6.

27. Zhang W, Trachootham D, Liu J, Chen G, Pelicano H, Garcia-Prieto C, et al. Stromal control of cystine metabolism promotes cancer cell survival in chronic lymphocytic leukaemia. Nat Cell Biol 2012;14:276–86.

28. Heider KH, Kuthan H, Stehle G, Munzert G. CD44v6: a target for antibody-based cancer therapy. Cancer Immunol Immunother 2004;53:567–79.

29. Boellaard R, Krak NC, Hoekstra OS, Lammertsma AA. Effects of noise, image resolution, and ROI definition on the accuracy of standard uptake values: a simulation study. J Nucl Med 2004;45:1519–27.

30. Hammond ME, Hayes DF, Dowsett M, Allred DC, Hagerty KL, Badve S, et al. American Society of Clinical Oncology/College Of American Pathologists guideline recommendations for immunohistochemical testing of estrogen and progesterone receptors in breast cancer. J Clin Oncol 2010;28:2784–95.

31. Bannai S. Exchange of cystine and glutamate across plasma membrane of human fibroblasts. J Biol Chem 1986;261:2256–63.

32. Tsai PJ, Huang PC. Circadian variations in plasma and erythrocyte concentrations of glutamate, glutamine, and alanine in men on a diet without and with added monosodium glutamate. Metabolism 1999;48:1455–60.

33. Park Y, Ziegler TR, Gletsu-Miller N, Liang Y, Yu T, Accardi CJ, et al. Postprandial cysteine/cystine redox potential in human plasma varies with meal content of sulfur amino acids. J Nutr 2010;140:760–5.

34. Steinink LD, Filer LJ Jr., Baker GL. Plasma glutamate concentrations in adult subjects ingesting monosodium L-glutamate in consomme. Am J Clin Nutr 1985;42:220–5.

Clinical Cancer Research

Exploratory Clinical Trial of (4S)-4-(3-[^{18}F]fluoropropyl)-l-glutamate for Imaging x$_C^-$ Transporter Using Positron Emission Tomography in Patients with Non−Small Cell Lung or Breast Cancer

Sora Baek, Chang-Min Choi, Sei Hyun Ahn, et al.

Updated version	Access the most recent version of this article at: doi:10.1158/1078-0432.CCR-12-0214
Supplementary Material	Access the most recent supplemental material at: http://clincancerres.aacrjournals.org/content/suppl/2012/08/13/1078-0432.CCR-12-0214.DC1

Cited articles	This article cites 34 articles, 18 of which you can access for free at: http://clincancerres.aacrjournals.org/content/18/19/5427.full#ref-list-1
Citing articles	This article has been cited by 12 HighWire-hosted articles. Access the articles at: http://clincancerres.aacrjournals.org/content/18/19/5427.full#related-urls

E-mail alerts	Sign up to receive free email-alerts related to this article or journal.
Reprints and Subscriptions	To order reprints of this article or to subscribe to the journal, contact the AACR Publications Department at pubs@aacr.org.
Permissions	To request permission to re-use all or part of this article, use this link http://clincancerres.aacrjournals.org/content/18/19/5427. Click on "Request Permissions" which will take you to the Copyright Clearance Center's (CCC) Rightslink site.